BIOCHEMISTRY
including biophysical chemistry & molecular biology

Article

pubs.acs.org/biochemistry

HYSCORE Analysis of the Effects of Substrates on Coordination of Water to the Active Site Iron in Tyrosine Hydroxylase

John McCracken,*[,†] Bekir E. Eser,[‡] Donald Mannikko,[†] Matthew D. Krzyaniak,[†] and Paul F. Fitzpatrick[‡]

[†]Department of Chemistry, Michigan State University, East Lansing, Michigan 48824, United States

[‡]Department of Biochemistry, University of Texas Health Science Center, San Antonio, Texas 78229, United States

Supporting Information

ABSTRACT: Tyrosine hydroxylase is a mononuclear non-heme iron monooxygenase found in the central nervous system that catalyzes the hydroxylation of tyrosine to yield L-3,4-dihydroxyphenylalanine, the rate-limiting step in the biosynthesis of catecholamine neurotransmitters. Catalysis requires the binding of tyrosine, a tetrahydropterin, and O_2 at an active site that consists of a ferrous ion coordinated facially by the side chains of two histidines and a glutamate. We used nitric oxide as a surrogate for O_2 to poise the active site iron in an $S = {}^3/_2$ {FeNO}^{7} form that is amenable to electron paramagnetic resonance (EPR) spectroscopy. The pulsed EPR method of hyperfine sublevel correlation (HYSCORE) spectroscopy was then used to probe the ligands at the remaining labile coordination sites on iron. For the complex formed by the addition of tyrosine and nitric oxide, TyrH/NO/Tyr, orientation-selective HYSCORE studies provided evidence of the coordination of one H_2O molecule characterized by proton isotropic hyperfine couplings (A_{iso} = 0.0 ± 0.3 MHz) and dipolar couplings (T = 4.4 and 4.5 ± 0.2 MHz). These data show complex HYSCORE cross peak contours that required the addition of a third coupled proton, characterized by an A_{iso} of 2.0 MHz and a T of 3.8 MHz, to the analysis. This proton hyperfine coupling differed from those measured previously for H_2O bound to {FeNO}^{7} model complexes and was assigned to a hydroxide ligand. For the complex formed by the addition of tyrosine, 6-methyltetrahydropterin, and NO, TyrH/NO/Tyr/6-MPH$_4$, the HYSCORE cross peaks attributed to H_2O and OH^- for the TyrH/NO/Tyr complex were replaced by a cross peak due to a single proton characterized by an A_{iso} of 0.0 MHz and a dipolar coupling (T = 3.8 MHz). This interaction was assigned to the N_5 proton of the reduced pterin.

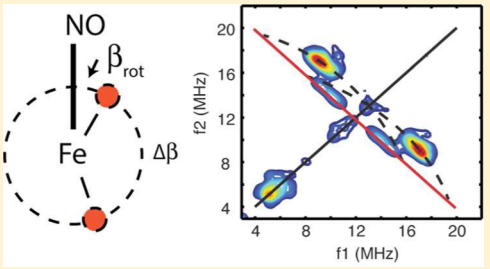

Tyrosine hydroxylase (TyrH) catalyzes the hydroxylation of substrate L-tyrosine (Tyr) to produce L-3,4-dihydroxyphenylalanine (L-DOPA), the rate-limiting step in the biosynthesis of the catecholamine neurotransmitters dopamine, epinephrine, and norepinephrine (Scheme 1). The enzyme is a member of a small class of enzymes known as aromatic amino acid hydroxylases that also catalyze the rate-limiting steps for the catabolism of phenylalanine, phenylalanine hydroxylase (PheH), and the biosynthesis of serotonin, tryptophan hydroxylase (TrpH).[1] Because the catecholamines are involved in the regulation of brain functions such as motor coordination, behavior, learning, and memory, dysfunction of TyrH has been linked to several neurological disorders.[2,3]

The overall reaction catalyzed by TyrH involves the coupled hydroxylations of a tetrahydropterin and Tyr, with an O_2 molecule supplying the oxygen atoms for each product. Catalysis occurs at a non-heme Fe(II) active site where the Fe is coordinated facially by the side chains of two histidines (His331 and His336) and one glutamate (Glu376), the so-called facial triad binding motif.[4,5] In the common mechanism proposed for all three aromatic amino acid hydroxylases, the reduced cofactor provides two electrons for the heterolytic cleavage of the O−O bond, leading to the formation of the 4a-hydroxypterin product and an Fe(IV)=O intermediate. Experimental evidence of an Fe(IV)=O intermediate in the catalytic cycle of TyrH has been provided by freeze-quench Mössbauer studies.[6] The Fe(IV)=O species then conducts hydroxylation of the aromatic side chain of the substrate amino acid via electrophilic aromatic substitution.[1] The binding of both the tetrahydropterin and the amino acid substrate to TyrH triggers a >100-fold enhancement of O_2 binding kinetics and is required for the formation of the Fe(IV)=O intermediate.[7] This requirement for binding of the substrate prior to oxygen activation appears to be a general mechanism for non-heme Fe oxygenases.[8]

The dramatic change in the reactivity of the iron site upon binding of both substrate and cofactor must be due to a change in the structure of the iron site. Structural and spectroscopic studies of TyrH and PheH have begun to provide insight into these structural changes. The original X-ray crystallographic structure [Protein Data Bank (PDB) entry 1TOH] for the catalytically inactive ferric TyrH in the absence of substrate and pterin showed the coordination geometry about the metal ion to be square pyramidal, with two histidines, a glutamate, and

Received: April 7, 2015
Revised: May 29, 2015
Published: May 29, 2015

DOI: 10.1021/acs.biochem.5b00363
Biochemistry 2015, 54, 3759−3771

Scheme 1. Hydroxylation Reactions Catalyzed by Tyrosine Hydroxylase

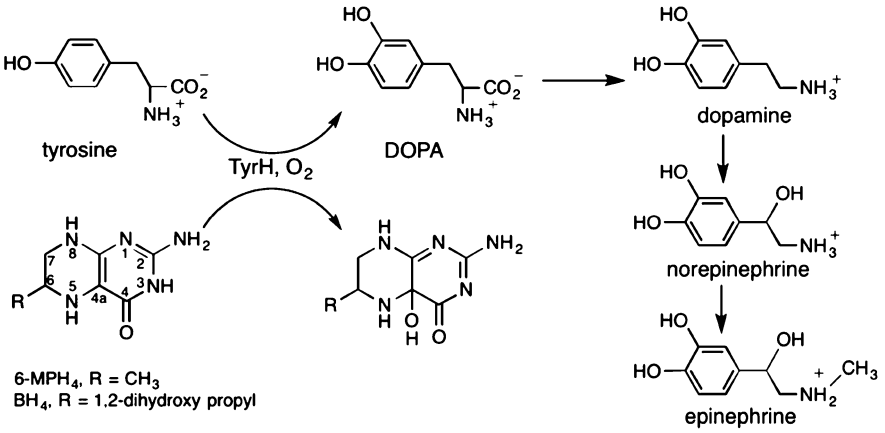

two water molecules as ligands.[4] X-ray absorption spectroscopy (XAS) and variable-temperature variable-field magnetic circular dichroism (VTVH MCD) studies of the catalytically relevant Fe(II) form of TyrH showed that the metal ion was six-coordinate with a distorted octahedral geometry in the resting state, consistent with three waters as ligands.[7] The addition of either Tyr or a tetrahydropterin to the Fe(II) enzyme resulted in only modest perturbations of the electronic structure of the six-coordinate Fe(II), indicating that neither reactant binds directly to the metal ion in the binary complexes. However, the binding of both Tyr and tetrahydropterin to the enzyme to form the O_2-reactive species gave rise to a structural change at the metal site, converting it from its six-coordinate resting form to a five-coordinate, square pyramidal site.[7] Spectroscopic results for this complex were most consistent with a single water molecule, two histidines, and a bidentate carboxylate acting as iron ligands.

Similar analyses with PheH provide complementary descriptions of the iron ligands in different enzyme−substrate complexes. The X-ray structure for the catalytic domain of PheH in the Fe(II) form in the absence of an amino acid substrate and a pterin (PDB entry 1J8T) shows facial coordination of the iron by the side chains of the two-histidine (His285 and His290), one-glutamate (Glu330) triad along with one well-ordered water ligand.[9] Because MCD studies of PheH in its resting state have shown that the Fe(II) is six-coordinate, it is presumed that there are three waters as ligands with the remaining two waters being disordered.[10] The X-ray crystal structure of a binary complex of truncated Fe(II) PheH with tetrahydrobiopterin (BH$_4$) (PDB entry 1J8U) clearly shows three water ligands in the open coordination positions of the active site Fe(II). The only amino acid residue with a side chain interacting with BH$_4$ is Glu286; the interaction occurs through two water molecules, one of which is a ligand to the metal. Glu286 and its counterpart in TyrH, Glu332, are essential for the coupled hydroxylation of substrates Phe and Tyr, respectively.[11,12] While attempts to crystallize ternary complexes of PheH with BH$_4$ and Phe have been unsuccessful, it has been possible to soak two "slow substrates", thienylalanine and norleucine, into binary crystals of PheH/BH$_4$, and the results showed substantial changes in the protein structure. Glu330 of the facial triad was reoriented so that it provided a bidentate coordination of its carboxylate side chain to Fe(II), and BH$_4$ was positioned closer to the Fe(II) with the distance between the metal ion and the C$_4$ oxygen of the cofactor decreasing from 3.8 to3.1 Å and with Glu286 forming direct hydrogen bonds with the pterin (PDB entry 1MMK).[13] One water molecule clearly remained as an iron ligand in the structure with norleucine, but not with thienylalanine. XAS, CD, and VTVH MCD studies of ternary complexes of intact rat Fe(II)-PheH with L-Phe and the air-stable 5-deaza-6-methyltetrahydropterin were most consistent with a five-coordinate, distorted square pyramidal geometry about the metal, suggesting that one water remains bound as a ligand in the ternary complex.[14] There are no X-ray crystal structures of either TyrH or PheH with only their amino acid substrates bound in the active site. For both enzymes, spectroscopic studies of the complexes with the amino acid bound are consistent with a six-coordinate site, with some perturbation from the unliganded enzymes.[7,15] Recently, density functional theory calculations based on the X-ray structures of PheH have suggested that the coordination sphere of the PheH/BH$_4$/L-Phe ternary complex is completed by coordination of the pterin through the C$_4$ carbonyl oxygen, leaving the Fe(II) with a distorted trigonal bipyramidal coordination geometry.[16]

For the resting forms of PheH and TyrH and for the tetrahydropterin-bound enzymes, the combination of structural and spectroscopic data to date supports a distorted octadedral iron site with three waters, two histidines, and a monodentate carboxylate as ligands. For the enzymes in which only the amino acid substrate is bound, the iron sites are still six-coordinate, but the number of waters and the nature of the glutamate interaction are unsettled. The greatest uncertainty is the identity of the fifth ligand in the O_2-reactive complex, with both water and the pterin proposed as ligands. This is an important issue to resolve for understanding the catalytic mechanism and the coupling of the hydroxylation reactions that comprise productive catalysis. Moreover, none of the studies to date address the structure of the complex formed when the ternary complex binds O_2, because it is too reactive. The formation of a five-coordinate site in the presence of both substrates suggests that a key factor in the reaction with oxygen is the formation of an open site due to the change in the coordination of the iron.

To address these issues, we have undertaken a series of one- and two-dimensional electron spin echo envelope modulation (ESEEM) experiments on TyrH treated with Tyr and 6-methyl-tetrahydropterin (6-MPH$_4$). To allow robust EPR detection of the catalytic center, the high-spin Fe(II) ion was treated with nitric oxide to form an $S = {}^3/_2$ {FeNO}^{7}

DOI: 10.1021/acs.biochem.5b00363
Biochemistry 2015, 54, 3759−3771

species.[17,18] This experimental approach to EPR studies of non-heme Fe(II) enzymes was pioneered by Lipscomb and Münck and offers unique opportunities for EPR structural studies.[19] Specifically, the use of NO as a surrogate for O_2 allows for the study of TyrH complexes prepared with catalytically competent substrate and cofactor. Furthermore, the anisotropy in the EPR spectrum coupled with the theoretically determined orientation of the Fe−NO bond with respect to the magnetic axes of the $\{FeNO\}^7$ paramagnetic center allows the magnetic couplings obtained from EPR/ESEEM studies to be interpreted in terms of the ligation structure about the metal ion.[20−22] Finally, previous Q-band ENDOR studies of $\{FeNO\}^7$ derivatives of 1-aminocyclopropane-1-carboxylate oxidase have shown that the isotropic ligand hyperfine couplings measured for the directly coordinated ^{14}N atoms of both histidine ligands and bound NO are small, 10−11 MHz, showing that very little unpaired electron spin density lies on the ligands.[23] As a consequence, distances derived from ^1H and ^2H dipolar couplings measured using ENDOR and ESEEM measurements of $\{FeNO\}^7$ derivatives of other non-heme Fe enzymes have compared well with available X-ray crystallographic structures.[23−26] If the coordination chemistry of NO truly mimics that of O_2, then the structural information gained from our studies has even greater relevance for understanding the catalytic mechanism. In a recent publication, we reported ^2H ESEEM studies of $\{FeNO\}^7$ complexes of TyrH prepared with ^2H-labeled tyrosine and 6-MPH_4. Our results showed that the binding of both substrate Tyr and cofactor 6-MPH_4 served to redirect NO binding to a coordination position that was essentially cis to that occupied for the TyrH/NO/Tyr sample.[27]

The work described here is aimed at characterizing coordination of water to Fe(II) for the TyrH/NO/Tyr ternary complex and the TyrH/NO/Tyr/6-MPH_4 quaternary complex and a TyrH variant, E332A/NO/Tyr/6-MPH_4, in which the reactive complex with oxygen forms but then decays to dihydropterin without the formation of Fe(IV).[7,27,28] Guided by a previous single-crystal ENDOR study of coordination of water to Cu(II) in Tutton salts, where large anisotropic proton hyperfine couplings were found,[29] we have made use of the unique capability of the four-pulse hyperfine sublevel correlation (HYSCORE) experiment to resolve broad ESEEM peaks and to separate them from the overlapping contributions due to additional ^1H and ^{14}N hyperfine couplings.[30,31] The results of these studies when combined with those obtained from our previous ^2H ESEEM measurements provide a more complete picture of the changes in the coordination chemistry that take place at the Fe(II) site of TyrH when the amino acid and pterin substrates bind.

EXPERIMENTAL PROCEDURES

Materials. 6-Methyltetrahydropterin (6-MPH_4) was purchased from Schircks Laboratories (Jona, Switzerland). 6-(2-Hydroxy-1-methyl-2-nitrosohydrazino)-*N*-methyl-1-hexanamine, ethylenediaminetetraacetic acid, L-tyrosine, and glycerol were from Sigma-Aldrich (St. Louis, MO). Potassium chloride and ferrous ammonium sulfate were from Fisher (Pittsburgh, PA). All other chemicals were of the highest purity commercially available. The preparation of NO complexes of wild-type and E332A TyrH expressed in *Escherichia coli* was described previously.[27]

EPR Spectroscopy. EPR measurements were taken on a Bruker E-680X spectrometer operating at X-band and equipped with a model ER 4118X-MD-X5-W1 probe that employed a 5 mm dielectric resonator. The temperature was maintained at 4.0 K using an Oxford Instruments liquid helium flow system equipped with a CF-935 cryostat and an ITC-503 temperature controller. ESEEM data were collected using a three-pulse (stimulated echo) sequence, 90°−τ−90°−T−90°, with 90° microwave pulse widths of 16 ns (fwhm). The τ values were chosen to suppress the ^1H matrix contribution; because of short phase memory times, they were restricted to <200 ns. Data were collected over a range of T values from 40 ns to just over 6 μs using a time increment of 12 ns and an integration window of 24 ns. A four-step phase cycling scheme was used to eliminate unwanted spin echoes and the DC offset voltage of the detection system from the data.[32] Normalized three-pulse ESEEM spectra were recorded by the division of a single-exponential background decay function prior to a processing procedure that involved removal of the DC component of the normalized modulation function by subtraction of a second-order polynomial, tapering with a Hamming window, zero filling of the data set to 1024 points, and, finally, Fourier transformation. Absolute value spectra are displayed in the figures.

HYSCORE data were collected using a four-pulse sequence, 90°−τ−90°−t_1−180°−t_2−90°, with all pulse widths set at 16 ns (fwhm).[33] Two pulse channels were used so that the peak power of the 90° pulses could be attenuated by 6 dB from that of the π pulse (approximately 800 W). The four-step phase cycle described by Gemperle et al.[34] for nonideal pulses was used for the same purpose as described above. HYSCORE data were collected using a 16 ns time increment with a 128 × 128 grid of data points being recorded. HYSCORE spectra were obtained from these data by subtraction of a second-order polynomial to remove the background decay in each time dimension, followed by application of a Hamming window, zero filling to yield a 256 × 256 data array, and two-dimensional FFT. The resulting absolute value spectra are displayed using contour plots with the plotting threshold set at 10−15% of the maximal peak amplitude.

EPR Analysis. The continuous wave (cw) EPR spectra of the $\{FeNO\}^7$ derivatives of TyrH studied in this work were analyzed in a previous study[27] using the "pepper" module of EasySpin 4.5.1[35] running in the MATLAB 2014a environment (The Mathworks, Natick, MA). These EPR spectra show nearly axial line shapes with features near g = 4 and g = 2. They are characteristic of $S = {}^3/_2$ paramagnetic centers where the EPR spectrum originates from the $m_s = \pm{}^1/_2$ Kramers doublet as a result of a large, positive spin−orbit coupling interaction. The spin Hamiltonian used to model these data consisted of a zero-field splitting term and an isotropic, spin-only, electronic Zeeman term with g_o = 2.00 (eq 1).

$$\hat{H} = D\left[\hat{S}_z^{\,2} - \frac{5}{4} + \frac{E}{D}(\hat{S}_x^{\,2} - \hat{S}_y^{\,2})\right] + g_o\beta_e\hat{\underline{S}}\cdot\underline{B} \qquad (1)$$

where β_e and $\underline{B}$ in eq 1 are the Bohr magneton and applied magnetic-field vector, respectively. D represents the zero-field splitting interaction and has been estimated from previous EPR, magnetic susceptibility, and Mössbauer studies of other NO-treated non-heme Fe^{2+} enzymes and $\{FeNO\}^7$ model complexes to be approximately 10 cm^{-1}.[19,36−38] Our previous analysis considered a fixed D value of 10 cm^{-1} and varied $|E|$, the strain in $|E|$, and the intrinsic EPR line width to fit the cw-EPR spectrum over an interval of 65 mT in the g = 4 region of the spectrum. The value of g_o in those simulations was used to

DOI: 10.1021/acs.biochem.5b00363
Biochemistry 2015, 54, 3759−3771

align the simulated spectra with the experimental data and was set to 2.02.

Proton HYSCORE spectra and three-pulse ESEEM spectra were analyzed using the "saffron" module of EasySpin 4.5.5.[39] For each proton considered in a simulation, the spin Hamiltonian that describes its ligand hyperfine coupling consists of nuclear Zeeman and electron−nuclear hyperfine coupling terms (eq 2).

$$\hat{H} = -\gamma_p \underline{\hat{I}} \cdot \underline{\mathbf{B}} + \underline{\hat{S}} \cdot \underline{\underline{\mathbf{A}}} \cdot \underline{\hat{I}} \tag{2}$$

where $\underline{\hat{I}}$ and $\underline{\hat{S}}$ in eq 3 are the nuclear and electron spin angular momentum operators, respectively, $\underline{\mathbf{B}}$ is the applied magnetic-field vector, and γ_p is the proton gyromagnetic ratio. $\underline{\underline{A}}$ is the hyperfine coupling matrix that has been transformed into the principal axis system (PAS) of the ZFS interaction.

Much of the HYSCORE and ESEEM analysis in this work is concerned with characterizing the hyperfine coupling of bound water molecules. Previous[29] single-crystal ENDOR studies of $Cu(H_2O)_6^{2+}$ showed that the proton hyperfine coupling of bound water molecules was primarily anisotropic in nature. For water ligands bound equatorially to Cu^{2+}, the isotropic or scalar portion of the proton hyperfine interaction was ≤1 MHz even though considerable unpaired spin density resided on the coordinated oxygen atom. The anisotropic portion of the proton hyperfine couplings had rhombic symmetry. For the axially bound water ligands of this complex, the isotropic proton hyperfine couplings were zero, and the anisotropic portion of the coupling had axial symmetry that was in line with values that could be predicted using the point dipole−dipole approximation. Recent ENDOR studies of {FeNO}^{7} adducts of the non-heme Fe enzyme 1-aminocyclopropane-1-carboxylic acid oxidase have shown that the isotropic ligand hyperfine couplings for the coordinated histidine nitrogens and the nitrogen atom of coordinated NO are approximately 10 MHz,[23] approximately 2−4 times weaker than the corresponding couplings measured for histidyl nitrogen coordinated equatorially to Cu(II) in proteins and model complexes.[40,41] Taken together, these results provided a framework for modeling the proton hyperfine coupling tensors for water molecules bound to Fe^{2+} in TyrH where the anisotropy in the coupling is modeled with a simple point dipole−dipole coupling, yielding a hyperfine tensor with principal values given by $(A_{iso} - T, A_{iso} - T, A_{iso} + 2T)$, where A_{iso} represents the isotropic coupling and

$$T = \left(\frac{\mu_o}{4\pi}\right)\frac{g_o g_n \beta_e \beta_n}{hr^3} \tag{3}$$

the dipolar coupling. The principal axis of the hyperfine tensor would be directed along a line connecting the Fe^{2+} with the coupled proton.

To be used in an ESEEM or HYSCORE simulation, the diagonal hyperfine tensor described above must be transformed into the principal axis system of the ZFS interaction. In EasySpin, this is done with a Euler transformation that uses a $zy'z'$ rotation scheme described by angles α, β, and γ, respectively. Because the hyperfine tensor has axial symmetry, only the β and γ angles need to be specified for each proton. In practice, specifying these angles was simplified because of the fixed geometric relationship between the two protons of a discrete water ligand, our prior knowledge of the facial bonding arrangement of the two-histidine, one-glutamate triad, and electronic structure calculations that place the principal axis of the ZFS interaction within 5° of the Fe−NO bond.[4,20] For our simulations, we adopted an elementary picture of the water molecule, with the oxygen atom being sp^3-hybridized and the ligand coordinating to Fe^{2+} through one of the oxygen lone electron pairs. Using this model, the protons could be located on the base of a cone, approximately 120° apart, with a symmetry axis that coincided with the Fe−OH_2 bond. Then, assuming an Fe^{2+}−O bond length of 2.1 Å, an O−H bond length of 1.0 Å, and a typical tetrahedral bond angle of 110°, the Euler angles needed to specify the transformations for both of the water protons were determined from the angles that orient the Fe(II)−OH_2 bond with respect to the ZFS axis system and a rotation angle that describes the orientation of the two protons about the bond axis. This approach to defining the hyperfine tensor transformation angles for the two protons of a bound water molecule is summarized in Scheme 2. It does not reduce the number of angles that need to be specified to transform the proton hyperfine tensors as one still must provide polar and azimuthal angles to position the Fe−O bond in the ZFS axis system, θ_{bond} and ϕ_{bond}, along with β_{rot} and $\Delta\beta$ to define the positions of the protons on the cone base (Scheme 2b). However, it makes it easier to visualize the transformations in terms of structure and to understand the limited range over which some of the angles need to be varied in simulations. The geometric relationships describing the transformations of the hyperfine tensors that need to be conducted for protons 1 and 2 of a bound water molecule having the geometry described above (Scheme 2) are given in eqs 4−7.

Scheme 2. Elementary Structure of a Water Ligand

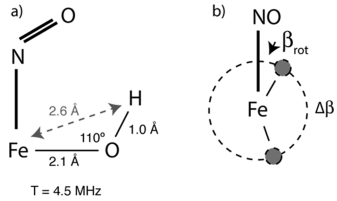

$$\beta_{hf1} = \theta_{bond} - \tan^{-1}[0.94 \times \cos(\beta_{rot})/2.42] \tag{4}$$

$$\gamma_{hf1} = \phi_{bond} - \tan^{-1}[0.94 \times \sin(\beta_{rot})/2.42] \tag{5}$$

$$\beta_{hf2} = \theta_{bond} - \tan^{-1}[0.94 \times \cos(\beta_{rot} + \Delta\beta)/2.42] \tag{6}$$

$$\gamma_{hf2} = \phi_{bond} - \tan^{-1}[0.94 \times \sin(\beta_{rot} + \Delta\beta)/2.42] \tag{7}$$

Because water ligands bound to Fe^{2+} are expected to be cis to the Fe−NO bond axis, the value of θ_{bond} should be close to 90°. The near axial symmetry of the cw-EPR spectrum reduces the importance of ϕ_{bond}, but if two water molecules are considered in a simulation, the ϕ_{bond} values should be close to 90° apart. Finally, the value of $\Delta\beta$ should fall in a range that is ±20° from our elementary starting value of 120°. In practice, the hyperfine couplings for the protons of a water ligand were specified in our simulations by providing discrete values for the dipolar couplings, $T^{(1)}$ and $T^{(2)}$, and a value for β_{rot}. The values of θ_{bond} (90°), ϕ_{bond} (0° or 90°), and $\Delta\beta$ (120°) were held constant.

RESULTS

TyrH/NO/Tyrosine Complex. To gain insight into the structure of the iron site in the TyrH/Tyr complex, HYSCORE analyses were conducted with the TyrH/Fe^{2+}/NO/Tyr

DOI: 10.1021/acs.biochem.5b00363
Biochemistry 2015, 54, 3759−3771

complex. The cw-EPR spectrum of the latter is shown in the inset of Figure 1a. The three-pulse ESEEM spectrum collected

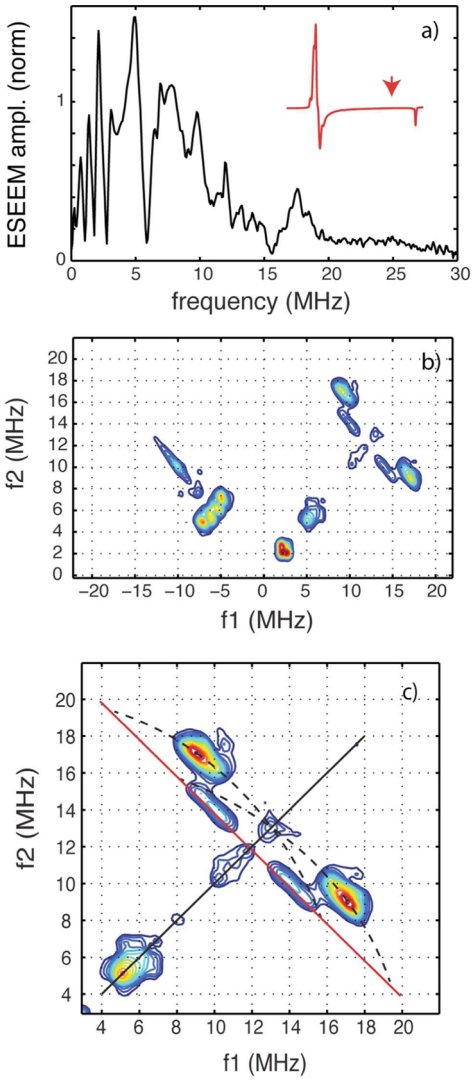

Figure 1. (a) Three-pulse ESEEM and (b and c) HYSCORE spectra of the TyrH/NO/Tyr complex. Data were collected using the following conditions: microwave frequency, 9.688 GHz; field strength, 280 mT; τ value, 84 ns; sample temperature, 4.0 K; pulse repetition rate, 1 kHz. For panel a, a 12 ns time increment was used and the data set length was 512 points. HYSCORE data were collected (b and c) with a 16 ns time increment and a 128 × 128 point data set. For panel c, the coupling ridges (dashed lines) were sketched onto the plot using a drawing program.

at 280 mT (g_{eff} = 2.5) is shown in Figure 1a. For reference, 280 mT is marked with a red arrow on the cw-EPR spectrum. This ESEEM spectrum shows numerous complex features that arise from overlapping ^{14}N and ^{1}H contributions from the directly coordinated ^{14}N atoms of the bound histidine side chains and coordinated NO, as well as strongly coupled ^{1}H's from the histidyl ligands and, most likely, bound water molecules. Because the isotropic hyperfine couplings of the directly bound ^{14}N atoms are much greater than the ^{14}N Larmor frequency of 0.86 MHz at 280 mT, their cross peaks are resolved in the (−, +) quadrant at (−4.9, 7.3) and (−5.4, 6.1) MHz in the corresponding HYSCORE spectrum (Figure 1b).[30,33] Note that each cross peak has a mirror image about the frequency diagonal. In this paper, we will refer to these pairs by specifying the cross peak that appears on the more positive side of the frequency diagonal with respect to f2. Because the hyperfine couplings for protons are generally expected to be smaller than the proton Larmor frequency, ω_p, of 11.9 MHz at 280 mT, their cross peaks are resolved in the (+, +) quadrant. Figure 1c shows an expanded view of this window from 3 to 22 MHz along each frequency axis. The proton contributions are symmetrically resolved about the frequency diagonal (solid black line in Figure 1c), near ω_p = 11.9 MHz. The red line perpendicular to the frequency diagonal and intersecting it at ω_p is termed the ^{1}H "anti-diagonal" and serves as a reference line for interpreting the data. Specifically, ^{1}H's that show large dipolar couplings, like those typical of bound water molecules, will give rise to cross peaks that follow a "ridge" or "arc"-like trajectory to the high-frequency side of the anti-diagonal. These ridges crest above the anti-diagonal in proportion to T^2/ω_p and approach the anti-diagonal at the extremes of the hyperfine tensor, from $\omega_p + A_\perp$ to $\omega_p + A_\parallel$ for one ridge and from $\omega_p - A_\perp$ to $\omega_p - A_\parallel$ for its mirror image about the frequency diagonal. For bound water molecules with A_{iso} = 0 and, therefore, hyperfine coupling principal values of $(-T, -T, 2T)$, these ridges will cross one another and approach the anti-diagonal line at $\omega_p - T$ and $\omega_p + 2T$ for one ridge and at $\omega_p + T$ and $\omega_p - 2T$ for the other.[42,43] The dashed black lines in Figure 1c were drawn as guides to help visualize these "coupling ridges". For an isotropic spin system, cross peak intensity would be detected along the entire length of the ridges.[44] However, for the $S = {}^3/_2$ {FeNO}^{7} spin system being studied here, cross peaks are expected at discrete positions along each ridge that are determined by the orientation of the coupled nucleus within the framework of the magnetic axis system.[21] The intense cross peak at (9.0, 17.1) MHz (Figure 1c) is well separated from the anti-diagonal, showing that it originates from a hyperfine interaction with a large anisotropic contribution and making it a likely candidate for assignment to a bound water molecule. Also shown in Figure 1c is a cross peak along the anti-diagonal that spans the frequency range from (9, 15) to (11,13) MHz; this can be assigned, in part, to ^{1}H hyperfine couplings of the histidyl imidazole ligands.

To characterize the ^{1}H hyperfine coupling(s) for the cross peak resolved at (9.0, 17.1) MHz in Figure 1c, HYSCORE experiments were performed at eight field positions across the EPR spectrum. Figure 2 shows the (+, +) quadrant for six spectra collected at 20 mT intervals from 200 to 300 mT. The data show that the cross peak attributed to a proton coupling with large anisotropy is first observed at 220 mT at (5.4, 16.4) MHz and exhibits a ridge trajectory toward the frequency diagonal as one proceeds to a higher magnetic field. At 240 mT, this correlation has moved to (6.5, 16.6) MHz and shows a wedge- or heart-shaped contour. This wedge-shaped cross peak is also observed at 260 and 280 mT with these correlations being resolved at (7.8, 16.8) and (9.0, 17.1) MHz, respectively. At 300 mT, this correlation is starting to convolve with the ^{1}H cross peaks along the ^{1}H anti-diagonal, but a portion is still resolved at (10.7, 16.8) MHz. In addition to the cross peaks that track along this coupling ridge, correlations arising from ^{1}H combination frequencies are observed at (10.1, 16.2) and (10.7, 16.8) MHz in the spectra recorded at 200 and 220 mT, respectively (Figure 2). These cross peaks consist of contributions from a difference combination frequency, $|\omega_\alpha - \omega_\beta|$, and a fundamental hyperfine coupling frequency, ω_β, and are a consequence of multiple ^{1}H couplings of similar strength

DOI: 10.1021/acs.biochem.5b00363
Biochemistry 2015, 54, 3759−3771

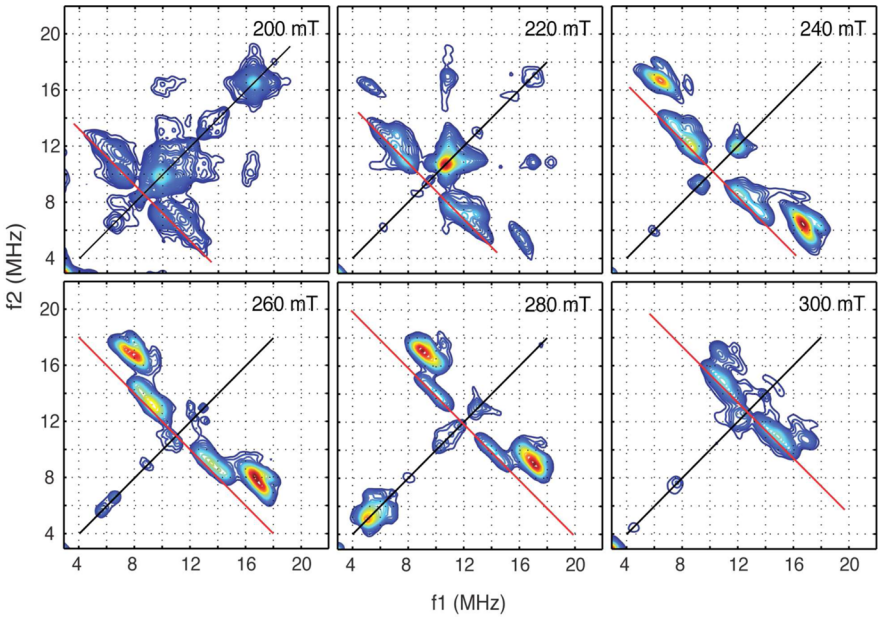

Figure 2. HYSCORE contour spectra collected for the TyrH/NO/Tyr complex under the conditions given in the caption for Figure 1. The τ values used for data acquisition were 116 ns at 200 mT, 108 ns at 220 mT, 96 ns at 240 mT, 92 ns at 260 mT, 84 ns at 280 mT, and 156 ns at 300 mT. Data are color-coded for intensity ranging from purple (weak) to red (strong).

associated with each $\{FeNO\}^7$ center. These data also show peaks along the frequency diagonal at (16.5, 16.5) MHz (200 mT) and (17.1, 17.1) MHz (220 mT) that arise from sum combination frequencies that are prominent in three-pulse ESEEM spectra collected near $g = 4$ and that contaminate these HYSCORE spectra.

The cross peaks that follow the "ridge" trajectory in Figure 2 were analyzed using the coupling model for the protons of a bound water molecule described in Experimental Procedures. Figure 3 shows expanded views of the wedge-shaped cross peaks resolved at 240, 260, and 280 mT (colored contours) along with HYSCORE simulations (red contours). The simulations shown in the left column were conducted for a single bound water molecule with Fe−OH_2 bond coordinates of $\theta_{bond} = 90°$ and $\phi_{bond} = 0°$ and water proton rotational locations of $\beta_{rot} = 48°$ and $\beta_{rot} + \Delta\beta = 168°$. For both water protons, the isotropic hyperfine coupling was set to zero. Dipolar couplings of 4.4 and 4.5 MHz were used for the protons located at $\beta_{rot} = 48°$ and $\beta_{rot} + \Delta\beta = 168°$, respectively. A full set of simulations using these parameters are compared to the data in Figure S1 of the Supporting Information. These simulations show that the simple model described by Scheme 2 does a good job of accounting for most of the cross peak intensity resolved at these three field positions. However, it fails to account for the wedge shape of the contours and also predicts additional strong cross peaks near (7.3, 13.7), (8.2, 14.2), and (9.2, 14.8) MHz at 240, 260, and 280 mT, respectively. These three additional cross peaks are near the $\omega_p \pm T$ frequency positions along the ^{1}H anti-diagonal and are expected, given the orientations of the coupled water protons with respect to the Fe−NO bond. However, the data show that the intensity of these features should be reduced in comparison to those of their wedge-shaped counterparts (Figure 2).

Attempts to account for these contour shapes by incorporating rhombic symmetry into the hyperfine coupling were unsuccessful. We also considered a model in which a second water ligand was added to the open coordination position on Fe. Simulations conducted using an A_{iso} of 0.0 and a T of 4.7 MHz for this second water were aimed at adding intensity to the region of the contour not covered by the one-water model and are shown in the right column of Figure S2 of the Supporting Information. The problem with this approach is that the second water yields cross peaks that are nearly parallel to those of the first so that the overall contour shape and the manner in which the composite cross peak coalesces as one moves to higher fields are less satisfactory.

The right side of Figure 3 shows that the data for the TyrH/NO/Tyr ternary complex can be accounted for by HYSCORE simulations (red) that consider one water ligand as described above along with a third proton introduced as a hydroxide ligand that occupies the other open coordination position *cis* to the Fe−NO bond. This third proton was characterized by $\theta_{bond} = 90°$, $\phi_{bond} = 90°$, and $\beta_{rot} = 34°$. To realize a "trajectory" for the cross peak contribution from this proton that resulted in a heart-shaped contour at 240 mT and collapsed into a wedge shape at 280 mT, an isotropic hyperfine coupling of 2.0 MHz and a dipolar coupling of 3.8 MHz were used for this simulation. This model also predicted additional cross peaks near the $\omega_p \pm T$ frequency positions along the ^{1}H anti-diagonal, but they are much weaker, as shown by the lower density of the red contours, and more in line with the data. A full set of HYSCORE simulations that use this three-proton model, or a one-H_2O, one-OH^- model, is shown in Figure 4. This model accounts for the coalescence of the ^{1}H cross peaks that occurs as one moves toward $g = 2.0$ (300 mT) and does a fair job of predicting the combination cross peaks at (10.1, 16.2) and (10.7, 16.8) MHz that are observed at 200 and 220 mT, respectively. The simulation of the HYSCORE data collected at 220 mT (Figure 4) shows a cross peak at (15.1, 17.3) MHz that arises from the third proton added to account for the wedge shapes of the cross peaks resolved from 240 to 280 mT. This cross peak was not resolved in our data. Because the predicted intensity of this extra peak is approximately half of that due to

DOI: 10.1021/acs.biochem.5b00363
Biochemistry 2015, 54, 3759−3771

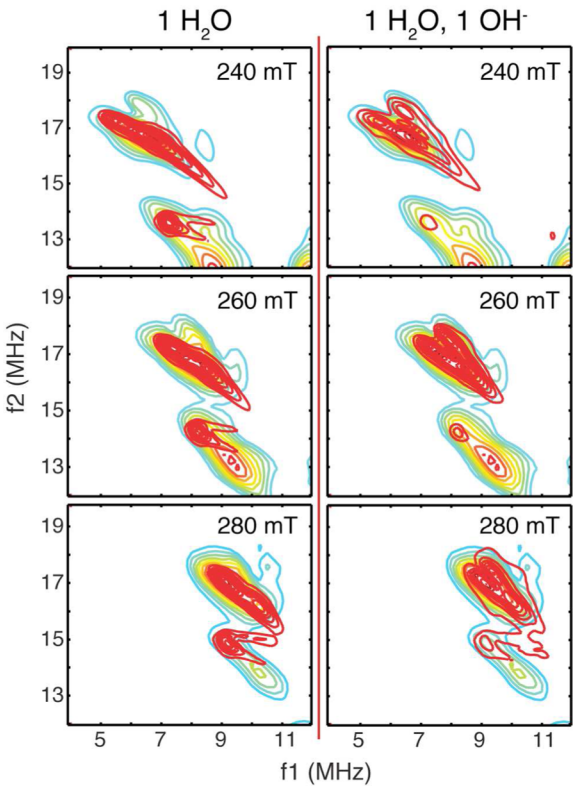

Figure 3. HYSCORE data (colored contours) and simulations (red contours) for the TyrH/NO/Tyr complex. The data are expansions of the spectra shown at 240, 260, and 280 mT in Figure 2. The simulations shown in the left column considered a single coordinated water molecule with ^{1}H hyperfine couplings given by (θ_{bond}, ϕ_{bond}) = (90°, 0°), β_{rot} = 48°, $\Delta\beta$ = 120°, ($T^{(1)}$, $T^{(2)}$) = (4.4,4.5) MHz, and $A_{iso}^{(1,2)}$ = 0.0 MHz. The simulations shown in the right column consider three protons with the first two being from water as specified for the left column, and the third one being described by (θ_{bond}, ϕ_{bond}) = (90°, 90°), β_{rot} = 34°, $T^{(3)}$ = 3.8 MHz, and $A_{iso}^{(3)}$ = 2.0 MHz. For both sets of simulations, a single $S = {}^3/_2$ paramagnetic center with D = 3.0 × 10^5 MHz, |E| = 5100 MHz, and g_o = 2.02 was considered.

the coupled water resolved at (5.4, 16.4) MHz at 220 mT, the discrepancy likely stems from a signal-to-noise issue.

TyrH/NO/Tyrosine/6-MPH$_4$ Complex. Figure 5 shows ^{1}H HYSCORE spectra obtained for the TyrH/NO/Tyr/6-MPH$_4$ quaternary complex. The cw-EPR spectrum is shown in the inset for the data collected at 240 mT. These HYSCORE spectra are markedly different from those of the ternary complex with tyrosine. The combination frequency cross peaks that were detected at (10.1, 16.2) and (10.7, 16.8) MHz at 200 and 220 mT, respectively, for the TyrH/NO/Tyr sample are absent from the data shown in Figure 5. The spectra do show evidence of at least one ^{1}H with a strong dipolar coupling. The coupling is different from those attributed to water and hydroxide for the TyrH/NO/Tyr complex, as cross peaks from the fundamental ^{1}H hyperfine coupling frequencies are resolved across the entire 200−300 mT range of magnetic-field values shown in Figure 5. At 200 mT, the cross peak shows a true ridge shape that extends from approximately (2.0, 15.8) MHz, where it meets the ^{1}H anti-diagonal, to (6.5,14.0) MHz. At 220 mT, this cross peak becomes shorter and is centered at (4.4, 15.9) MHz. As one goes to higher-field values, the cross peaks become better resolved as they move toward the frequency diagonal. These higher-field cross peaks are resolved at (5.9, 16.1), (7.4, 16.5), (9.2, 16.5), and (10.9, 16.4) MHz at 240, 260, 280, and 300 mT, respectively. Control experiments conducted with samples in ^{2}H$_2$O showed that the proton that gives rise to these cross peaks is exchangeable (Figure S3 of the Supporting Information). Simulations of these features of the ^{1}H HYSCORE spectra were accomplished considering a single ^{1}H coupled through space with a dipolar coupling of T = 3.8 MHz and coupling tensor Euler angles of β_{hf} = 68° and γ_{hf} = 90°. These simulations are shown in red, overlaid on the data, in Figure 6.

Proton HYSCORE measurements were also performed on the quaternary complex of a TyrH variant, E332A/NO/Tyr/6-MPH$_4$. These data were identical to those collected for the quaternary complex of the wild-type enzyme and are shown in Figure S4 of the Supporting Information.

DISCUSSION

Here we have used ^{1}H HYSCORE spectroscopy to extend our previous analyses of NO complexes of TyrH to characterize Fe(II) ligation in the TyrH/NO/Tyr complex, an analogue of the TyrH/Tyr complex that has not been amenable to crystallization, and the TyrH/NO/Tyr/6-MPH$_4$ complex, a model for the reactive quaternary TyrH/O$_2$/Tyr/6-MPH$_4$ complex. In both cases, the results provide new insights into the structure of these otherwise inaccessible intermediates.

For the TyrH/NO/Tyr complex, our data showed cross peaks with a complex contour shape that were observed over a limited range of the EPR spectrum, from 220 mT (g = 3.1) to 300 mT (g = 2.3), and well separated from the ^{1}H anti-diagonal (Figure 2). In addition to these correlations between fundamental ^{1}H hyperfine coupling frequencies, (ω_α, ω_β), cross peaks that could be attributed to combination frequencies of the form ($|\omega_\alpha - \omega_\beta|$, ω_β) were observed at 200 and 220 mT (Figure 2). These combination frequencies are diagnostic for the participation of multiple nuclei in this particular hyperfine interaction. We initially analyzed these HYSCORE cross peaks using a simple model for a single bound water. Simulations considering a single water molecule coordinated to the {FeNO}^{7} center with hyperfine couplings described by (θ_{bond}, ϕ_{bond}) = (90°, 0°), A_{iso} = 0.0 MHz, ($T^{(1)}$, $T^{(2)}$) = (4.4, 4.5) MHz, β_{rot} = 48°, and $\Delta\beta$ = 120° (Figure 3 and Figure S1 of the Supporting Information) show that this model accounts well for the combination frequency cross peaks observed at lower fields. Simulations that considered A_{iso} to be in the range of 0.5−1.0 MHz were unsatisfactory for several reasons. At 200 and 220 mT, they failed to properly account for the combination frequency cross peak positions. In the range of 220−240 mT, they predicted intensity ratios for the two "lobes" of the heart-shaped contours of equal intensity, and at 300 mT, these simulations could not account for the position or shape of the cross peak resolved at (10.7, 16.8) MHz. These deficiencies were used to place a limit of ±0.3 MHz on the A_{iso} value for the water protons.

These experimental observations and the ^{1}H hyperfine coupling parameters derived from their analysis are nearly identical to those measured for water bound to a series of model complexes of the type {FeNO}^{7}(N$_2$O$_x$)(H$_2$O)$_{x-3}$, where x = 1−3. These model complexes were based on a ligand that was developed to mimic the N$_2$O core of the facial triad and could be modified with the addition of acetate groups to make it tridentate (N$_2$O), tetradentate (N$_2$O$_2$), and pentadentate (N$_2$O$_3$). As a result, the NO and water ligands are *cis* to one

DOI: 10.1021/acs.biochem.5b00363
Biochemistry 2015, 54, 3759−3771

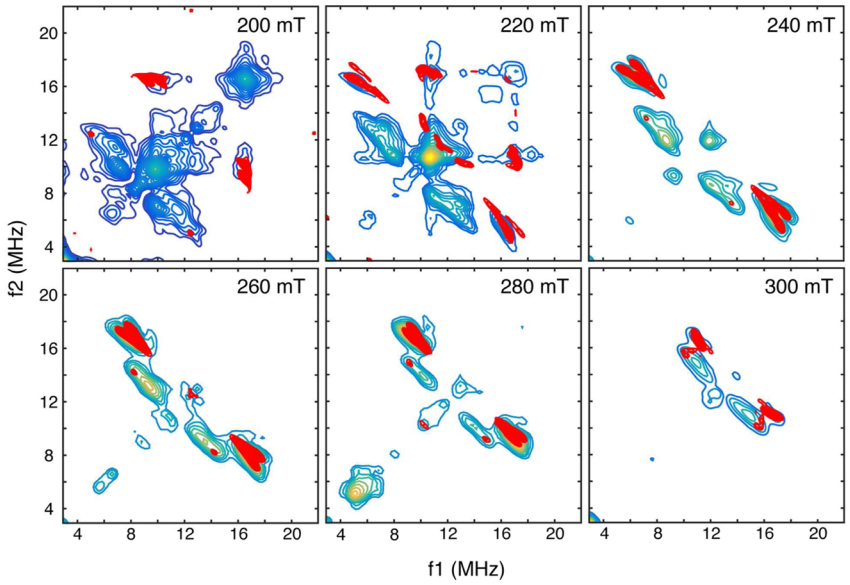

Figure 4. HYSCORE data (colored contours) compared to simulations (red contours) for the full data set shown in Figure 2. The simulations were conducted using a three-proton model considering one water ligand described by $(\theta_{bond}, \phi_{bond}) = (90°, 0°)$, $\beta_{rot} = 48°$, $\Delta\beta = 120°$, $(T^{(1)}, T^{(2)}) = (4.4, 4.5)$ MHz, and $A_{iso}^{(1,2)} = 0.0$ MHz and one hydroxide ligand described by $(\theta_{bond}, \phi_{bond}) = (90°, 90°)$, $\beta_{rot} = 34°$, $T^{(3)} = 3.8$ MHz, and $A_{iso}^{(3)} = 2.0$ MHz. For both sets of simulations, a single $S = {}^3/_2$ paramagnetic center with $D = 3.0 \times 10^5$ MHz, $|E| = 5100$ MHz, and $g_o = 2.02$ was considered.

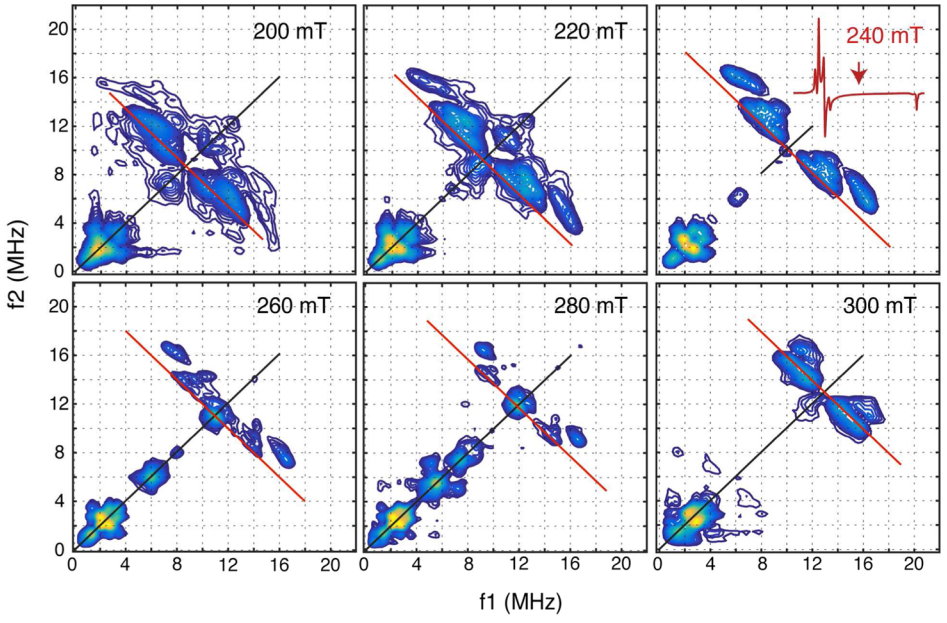

Figure 5. HYSCORE spectra of the TyrH/NO/Tyr/6-MPH_4 complex. Data were collected under the following conditions: microwave frequency, 9.687 GHz; sample temperature, 4.0 K; time increment, 16 ns; pulse sequence repetition rate, 1 kHz; data set dimensions, 128 × 128; and τ values, 116 ns at 200 mT, 108 ns at 220 mT, 96 ns at 240 mT, 92 ns at 260 mT, 84 ns at 280 mT, and 156 ns at 300 mT. The contours are color-coded for intensity ranging from purple (weak) to red (strong).

another for both $\{FeNO\}^7(N_2O)(H_2O)_2$ and $\{FeNO\}^7(N_2O_2)(H_2O)$ complexes.[45] HYSCORE experiments performed on these complexes showed that water bound to the $\{FeNO\}^7$ center was characterized by an A_{iso} of 0.0 ± 0.3 MHz and dipolar coupling values, T, that ranged from 4.6 to 4.9 MHz. Furthermore, these studies mirrored those presented here for TyrH in that cross peaks arising from the fundamental ^{1}H hyperfine frequencies were resolved over only a limited range of magnetic-field strengths from 220 to 300 mT, while correlations arising from combination frequencies were observed at lower fields.[46]

However, the simulations based on a single coordinated water (left sides of Figure 3 and Figure S2 of the Supporting Information) differ from the data in two important respects. The most obvious shortcoming is that they fail to account for the wedge shape of the cross peak contours that are resolved from 240 to 280 mT. The best way to account for the wedge shape and its magnetic-field dependence was to add a third proton to the simulation and to include an isotropic contribution to its hyperfine coupling to distinguish the trajectory of its coupling ridge from those attributed to water. These adjustments yielded an A_{iso} of 2.0 MHz along with a

DOI: 10.1021/acs.biochem.5b00363
Biochemistry 2015, 54, 3759−3771

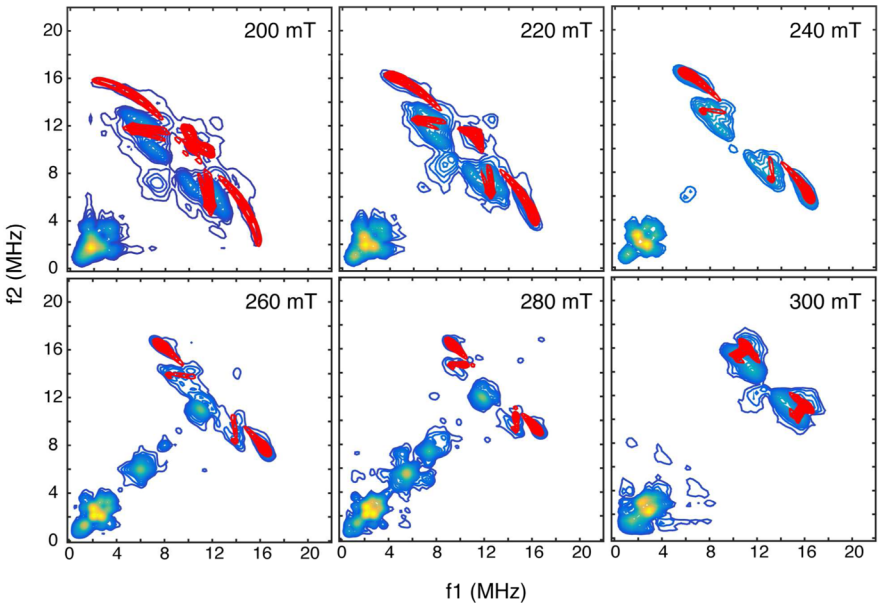

Figure 6. HYSCORE spectra recoded for the TyrH/NO/ty/6-MPH$_4$ complex (colored contours) compared to HYSCORE simulations (red contours). The data are identical to those shown in Figure 5, and the simulations consider a single proton described by the hyperfine couplings: β_{hf} = 68°, γ_{hf} = 90°, T = 3.8 MHz, and A_{iso} = 0.0 MHz. The simulations considered the paramagnetic center to be a mixture of two species with D = 3.0 × 10^5 MHz, $|E|^{(1)}$ = 6000 MHz (60% of the signal amplitude), $|E|^{(2)}$ = 15000 MHz (40% amplitude), and g_o = 2.02. The results of simulations conducted for each species were added to yield the red contours in the figure.

reduced dipolar coupling T of 3.8 MHz. This value of A_{iso} is double those reported for water molecules bound equatorially to Cu(II) in the Tutton salts,[29] and its non-zero value distinguishes it from the water molecules bound to the $S = {}^3/_2$ paramagnetic centers of the $\{FeNO\}^7(N_2O)(H_2O)_2$ and $\{FeNO\}^7(N_2O_2)(H_2O)$ model complexes.[46] Given its labile nature and what we know about the structure of the Fe site from X-ray crystallographic studies, we assigned these couplings to a hydroxide ligand. We used the framework developed above for bound water to specify the Euler angles needed to orient the axial proton hyperfine coupling tensor of OH^- and found that (θ_{bond}, ϕ_{bond}) = (90°, 90°) and β_{rot} = 34° yielded satisfactory simulations (Figure 3, right column).

Our assignment of these distinct coupling values to hydroxide is supported by a detailed spectroscopic characterization of Hg-substituted *Rhus vernicifera* laccase, in which a strongly coupled, exchangeable proton associated with the type 2 Cu(II) site was assigned to a hydroxide ligand. While the hyperfine couplings of the hydroxide proton were not determined, these authors reported a Q-band ^{2}H ENDOR spectrum of ^2H_2O-exchanged enzyme and used it as evidence of a strong exchangeable proton coupling.[47] Scaling our ^{1}H hyperfine coupling values (A_{iso} = 2.0 MHz, and T = 3.8 MHz) to ones appropriate for deuterium and using the experimental conditions given for the laccase work, we performed an ENDOR simulation for comparison with the published spectra for the ^2H_2O-exchanged type 2 Cu(II) site. Our simulated spectrum (Figure S5 of the Supporting Information) shows a frequency width between the low- and high-frequency shoulders of 1.5 MHz that compares well with the value of 1.4 MHz measured from the laccase data.

The second shortcoming of the single-water model concerns the relative intensities of the cross peaks predicted along each coupling ridge over the field range of 220−300 mT in Figure 3 and Figure S2 of the Supporting Information. Specifically, for a single coupled water bound *cis* to NO, HYSCORE simulations show cross peaks at four positions along each coupling ridge. The cross peaks predicted at (5.6, 17.2) and (6.8, 16.6) MHz at 240 mT (Figure 3, top left simulations) are positioned at orientation-averaged values weighted by $A_{||}$ and $A_{\perp}$ for both protons and are associated with the canonical orientation of the ZFS tensor that lies along the Fe−OH_2 bond. In contrast, the cross peak predicted at (7.3, 13.5) MHz originates from the ZFS canonical orientation perpendicular to the Fe−OH_2 bond where the orientation-averaged coupling is weighted almost entirely by $A_{\perp}$ for both protons. Because the dispersion in the $A_{\perp}$ values is small, only a single cross peak is predicted near the $\omega_p \pm A_{\perp}$ position along the anti-diagonal, and its intensity, which can be judged by the density of contours, is comparable to those resolved at (5.6, 17.2) and (6.8, 16.6) MHz. When the hydroxide or a second water is added, it must be positioned at the other open coordination position yielding a *fac* arrangement for NO, H_2O, and OH^-/H_2O. The orientation averaging now samples the full extent of the hyperfine tensor for at least one proton at both of the canonical orientations mentioned above. The simulations for the one-H_2O, one-OH^- model consider all three protons simultaneously, and the resulting HYSCORE product functions show a loss of intensity for the cross peaks resolved at the $\omega_p \pm A_{\perp}$ positions along each ridge. These simulations (right side of Figure 3 and Figure S2 of the Supporting Information) reveal relative cross peak intensities that are in better agreement with the HYSCORE data of Figure 2. We conclude that the TyrH/NO/Tyr ternary complex has both water and hydroxide ligands bound to its open coordination sites and that the carboxylate side chain of Glu376 retains its monodentate coordination to Fe(II). The TyrH/Tyr complex would then have as ligands two histidines, a monodentate glutamate, two waters, and one hydroxide.

The difference in hyperfine couplings measured for the water ligand [A_{iso} = 0.0 ± 0.3 MHz; ($T^{(1)}$, $T^{(2)}$) = 4.4, 4.5 ± 0.2 MHz] and hydroxide (A_{iso} = 2.0 MHz; T = 3.8 MHz) could stem from their structural relationship with the NO ligand.

DOI: 10.1021/acs.biochem.5b00363
Biochemistry 2015, 54, 3759−3771

Electronic structure calculations have shown that the $S = {}^3/_2$ $\{FeNO\}^7$ center is best viewed as an $S = {}^5/_2$ Fe^{3+} antiferromagnetically coupled to an $S = 1$ NO^-.[37,48] Recently, Silakov and co-workers have used a distributed spin model based on this electronic structure to interpret ^2H hyperfine couplings they obtained from Q-band HYSCORE studies of $\{FeNO\}^7$ derivatives of a 2-ketoglutarate-dependent halogenase, SyrB2.[49] Because the unpaired electron spin on the NO is of opposite sign, a proton closely associated with the oxygen atom of NO would be expected to show a dipolar coupling smaller than those at a greater distances. Figure 7a shows a

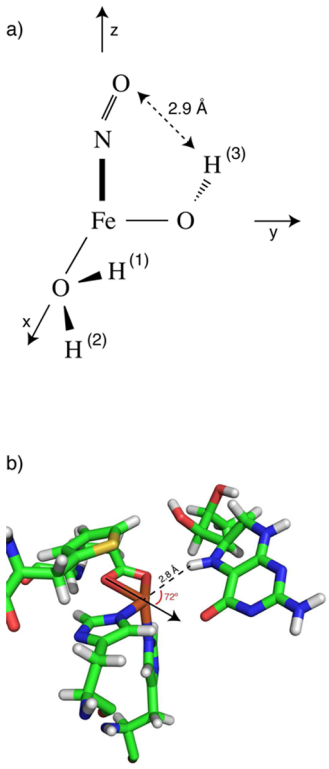

Figure 7. (a) Stick structure showing the proposed relationship between the $\{FeNO\}^7$ center of the TyrH/NO/Tyr ternary complex and the coordinated water and hydroxide ligands. The Fe−OH^-, Fe−OH_2, and Fe−NO bond lengths were 2.1, 2.1, and 1.75 Å, respectively. The N═O bond length was 1.15 Å, and the Fe−N−O bond angle was 160°. β_{rot} angles for the proton orientations were 34°, 48°, and 168° for $H^{(3)}$, $H^{(1)}$, and $H^{(2)}$, respectively. (b) Active site of PheH cocrystallized with BH_4 and soaked with thienylalanine, a "slow substrate" (PDB entry 1MMK). The black arrow was drawn along one of the Fe^{2+}−O bonds to the glutamate ligand and is proposed as the bond axis for NO ligation. Taking this arrow as the z-axis of the magnetic coordinate system, we find the polar angle that describes the orientation of N_5 ^1H of the pterin is 72° and the distance from Fe to this proton is 2.8 Å. H atoms were drawn on this structure using MacPyMol, and the angle and distance were measured with this program, as well.

proposed structure for the arrangement of the NO, OH^-, and H_2O ligands coordinated to the active site Fe. In this structure, the atoms of the $\{Fe\text{-}NO\}^7$ center are coplanar with the Fe−OH^- bond. The β_{rot} angles obtained from our HYSCORE simulations, 34° for the hydroxide proton and 48° and 168° for the water protons, were used to orient the ligand protons. Considering Fe−OH^- and Fe−OH_2 bonds to be 2.1 Å (Scheme 2) and using an Fe−NO structure commensurate with those reported for several model complexes (Fe−N bond, 1.75 Å; N−O bond, 1.15 Å; Fe−N−O bond angle, 160°), the hydroxide proton, $H^{(3)}$, is found to be nearly equidistant from Fe and N, 2.6 Å, and just 2.9 Å from the oxygen atom of NO.[37,50,51] Using the model provided by Silakov and co-workers, the dipolar coupling for $H^{(3)}$ was predicted to be 4.7 MHz.[49] Repeating this calculation for the protons of the water ligand where the distances to the NO oxygen are 3.8 Å [$H^{(1)}$] and 4.5 Å [$H^{(2)}$], one obtains dipolar couplings of 5.0 and 5.6 MHz, respectively. While these predicted couplings are larger than those measured in this study, they predict that the dipolar coupling for the hydroxide proton [$H^{(3)}$] will be 0.9 MHz lower than the coupling for $H^{(2)}$ of the water ligand. This predicted difference is within experimental error of the value of 0.7 MHz reported here.

The ^1H HYSCORE spectra recorded for the TyrH/NO/Tyr/6-MPH_4 quaternary complex differ from those of the TyrH/NO/Tyr complex in several respects. Correlations arising from the fundamental proton hyperfine frequencies of a ^1H with a large dipolar coupling were observed across the entire range from 200 to 300 mT of magnetic-field values (Figure 5). The fundamental and combination frequency cross peaks seen in the TyrH/NO/Tyr complex are absent from spectra collected for the TyrH/NO/Tyr/6-MPH_4 complex. No combination peaks are observed at the lower fields, indicating that these cross peaks originate from a single proton. Our analysis was based on a single proton characterized by hyperfine couplings of $A_{iso} = 0.0$ MHz, $T = 3.8$ MHz, and Euler rotation angles of $\beta_{hf} = 68°$ and $\gamma_{hf} = 90°$ (Figure 6). These couplings are distinct from those reported above for the ternary complex with Tyr. Figure S6 of the Supporting Information shows an overlay of the simulations conducted for the TyrH/NO/Tyr (black) and TyrH/NO/Tyr/6-MPH4 (red) enzyme complexes. The quaternary complex yields cross peaks that trace a coupling ridge as a function of field strength that is very different from the two ridges that characterize the TyrH/NO/Tyr complex. The absence of combination cross peaks and the smaller dipolar coupling, in comparison to those found for the ternary complex and for $\{FeNO\}^7$ model complexes, rules out the possibility that this coupling originates from bound water.[46] While the dipolar coupling is identical to that attributed to a hydroxide ligand for the ternary complex, the A_{iso} value of 0.0 MHz serves to distinguish it.

We previously found[27] that the cw-EPR spectrum of the TyrH/NO/Tyr complex was consistent with more than 90% of the $S = {}^3/_2$ EPR signal arising from a single paramagnetic species characterized by $|E|/D = 0.017$, with the remaining 10% of the signal featuring a rhombicity in the ZFS interaction of $|E|/D = 0.04$. In contrast, the data for the wild-type and E332A TyrH/NO/Tyr/6-MPH_4 complexes suggested that each was a composite of two paramagnetic species, a major component with $|E|/D = 0.02$ that accounted for 60% of the EPR signal amplitude, and a minor component with $|E|/D = 0.05$. Both species showed comparable strains in $|E|$. For the analysis of ^2H ESEEM data, it was assumed that NO coordinated to Fe at the same position relative to the ligands of the facial triad for both species and that the modest difference in $|E|/D$ arose from different rotational conformations of NO about the Fe−NO bond, and/or different Fe−N−O bond angles.[27,48,52] While this interpretation had been adopted previously for EPR studies of $\{FeNO\}^7$ adducts of a bacterial PheH,[53] it cast doubt on the ^2H ESEEM analysis as the hyperfine couplings that were analyzed in that study were weak so that the spectra had few

DOI: 10.1021/acs.biochem.5b00363
Biochemistry 2015, 54, 3759−3771

distinguishing features. The resolution of the HYSCORE data presented in Figure 5 for the TyrH/NO/Tyr/6-MPH_4 adduct and, more specifically, the resolution of the coupling ridges for the proton characterized by the 3.8 MHz dipolar coupling strengthen the argument that NO is bound to Fe at a unique position with respect to the other ligands of the facial triad. It would be fortuitous for a mixture, especially one characterized by a 60/40 speciation, to give rise to a single set of cross peaks across the entire width of the EPR spectrum.

Previous ^2H ESEEM studies of the quaternary complex of TyrH prepared with 3,5-$^2H_2$-Tyr and 6-MPH_4 showed a dipolar distance between the substrate and the $\{FeNO\}^7$ center of 4.7 ± 0.2 Å and an orientation for this coupling vector of 86 ± 10° with respect to the Fe−NO bond axis. For quaternary TyrH complexes prepared with 6,7-$^2H_2$-6-MPH_4, the effective distance to the closest deuteron was found to be 4.4 ± 0.2 Å with the coupling vector making a 66 ± 5° angle with the Fe−NO bond.[27] These data were interpreted structurally within the framework of the crystal structure obtained for the catalytic domain of PheH cocrystallized with tetrahydrobiopterin and soaked with thienylalanine (Figure 7b, PDB entry 1MMK). Assuming that substrate Tyr is bound at the active site in a fashion similar to that of thienylalanine, we concluded that NO must coordinate to Fe so that it is *cis* to the histidyl ligands and *trans* to one of the carboxylate oxygen atoms of the glutamate residue. Figure 7b shows this structure with an arrow drawn to represent the proposed direction for the Fe−NO bond. Coordination of NO in this fashion would provide a five-coordinate quaternary complex in agreement with the results of VTVH MCD studies and account for the absence of water and hydroxide ligands commensurate with our HYSCORE results.[7] The closest exchangeable ^1H would be the N_5 ^1H of the pterin. Placing protons into the crystal structure and evaluating the orientation of the pterin N_5 proton with respect to the proposed orientation of the Fe−NO bond yield an Fe−^1H distance of 2.8 Å and an orientation angle of 72°. The strongly coupled exchangeable proton detected in our HYSCORE measurements was characterized by a dipolar coupling of 3.8 MHz and an orientation of the hyperfine tensor principal axis with respect to the Fe−NO bond given by β_{hf} = 68°. The dipolar coupling value translates into a dipolar distance of 2.7 Å (eq 3). Given this agreement, we assign this coupling to the N_5 proton of the 6-MPH_4 cofactor.

NO is typically thought to bind as an O_2 analogue in spectroscopic and structural studies of non-heme iron proteins. A pentacoordinate TyrH iron complex containing NO thus suggests that binding of O_2 to the pentacoordinate complex with Tyr and pterin displaces the remaining water to form a pentacoordinate O_2 complex. This is in contrast to a model in which formation of a pentacoordinate complex opens up a site for oxygen to bind. It is not possible to rule out the possibility that the binding of NO in a stable complex differs from the binding of O_2 to an unstable and transiently formed catalytic intermediate. Still, the NO complex of TyrH provides a unique probe of the structural changes that occur in the active site that are required for a productive reaction with O_2.

Finally, ^1H HYSCORE spectra of the quaternary complex of the TyrH variant E332A were identical to those obtained for the wild-type enzyme. This mutant protein is representative of a large number of mutants of both TyrH and PheH in its uncoupling of tetrahydropterin oxidation from amino acid hydroxylation. These results are in agreement with the conclusions from a previous study[27] that the uncoupling of tyrosine hydroxylation from the pterin oxidation chemistry that results from this mutation is not due to an inability to form the reactive complex with oxygen. Rather, it is likely due to active site altered dynamics resulting from the loss of the stabilizing interaction between the pterin and Glu332. These altered dynamics would result in an unproductive decay of the quaternary complex of Tyr, tetrahydropterin, and O_2. Less complete studies of other aromatic amino acid hydroxylase mutants suggest that uncoupling can occur at multiple steps prior to addition of oxygen to the amino acid substrate. S395A TyrH forms the HO-pterin product with the same k_{cat} value as the wild-type enzyme, but the hydroxylation of Tyr by this enzyme is 99% uncoupled from tetrahydropterin oxidation.[54] Spectroscopic studies of complexes of two PheH mutants that also exhibit uncoupling established that the R158Q enzyme could still form a pentacoordinate complex in the presence of phenylalanine and the air-stable 5-deaza-6-methyl-tetrahydropterin, but that the iron in the E280K enzyme remained hexacoordinate.[55] Both of these residues are located outside of the PheH active site, unlike Glu332 and Ser395 in TyrH. This sensitivity of the coupling of tetrahydropterin oxidation, oxygen activation, and amino acid hydroxylation illustrates that catalysis of a productive reaction by this family of non-heme enzyme monooxygenases requires exquisitely fine-tuning of the protein structure.

SUMMARY

The results presented in this study show that the labile coordination sites at the Fe(II) catalytic center of TyrH treated with substrate Tyr and poised in an $S = {}^3/_2$ state by the addition of NO are occupied by the *fac* coordination of NO, H_2O, and OH^-. The addition of 6-MPH_4 to produce the TyrH/NO/Tyr/6-MPH_4 quaternary complex leads to the displacement of both water and hydroxide ligands and gives rise to a new ^1H hyperfine coupling that was distinguished in HYSCORE measurements. This new coupling can be assigned to N_5 ^1H of reduced pterin using a framework provided by X-ray crystallographic studies of PheH and previous ESEEM studies of TyrH.

ASSOCIATED CONTENT

Supporting Information

HYSCORE spectra and spectral simulations to support the material presented in Results and interpretations of the data presented in Discussion. The Supporting Information is available free of charge on the ACS Publications website at DOI: 10.1021/acs.biochem.5b00363.

AUTHOR INFORMATION

Corresponding Author

*E-mail: mccracke@msu.edu. Phone: (517) 355-9715. Fax: (517) 353-1793.

Funding

This work was supported in part by Grant CHE-1404129 from the National Science Foundation (P.F.F.) and Grant AQ-1245 from The Welch Foundation (P.F.F.). The EPR instrument was purchased with funds supplied by the National Institutes of Health (Grant S10 RR15880) (J.M.) and the Michigan Economic Development Corp.

Notes

The authors declare no competing financial interest.

DOI: 10.1021/acs.biochem.5b00363
Biochemistry 2015, 54, 3759−3771

■ ABBREVIATIONS

TyrH, tyrosine hydroxylase; PheH, phenylalanine hydroxylase; BH_4, tetrahydrobiopterin; 6-MPH_4, 6-methyltetrahydropterin; L-DOPA, L-3,4-dihydroxyphenylalanine; Tyr, tyrosine; EPR, electron paramagnetic resonance; ESEEM, electron spin echo envelope modulation; hf, hyperfine; HYSCORE, hyperfine sublevel correlation; PAS, principal axis system.

■ REFERENCES

(1) Fitzpatrick, P. F. (2003) Mechanism of Aromatic Amino Acid Hydroxylation. *Biochemistry 42*, 14083−14091.

(2) Zafeiriou, D. I., Willemsen, M. A., Verbeek, M. M., Vargiami, E., Ververi, A., and Wevers, R. (2009) Tyrosine Hydroxylase Deficiency with Severe Clinical Course. *Mol. Gen. Metab. 97*, 18−20.

(3) Royo, M., Daubner, S. C., and Fitzpatrick, P. F. (2005) Effects of Mutations in Tyrosine Hydroxylase Associated with Progressive Dystonia on the Activity and Stability of the Protein. *Proteins 58*, 14−21.

(4) Goodwill, K. E., Sabatier, C., Marks, C., Raag, R., Fitzpatrick, P. F., and Stevens, R. C. (1997) Crystal Structure of Tyrosine Hydroxylase at 2.3 Å and its Implications for Inherited Neurodegenerative Diseases. *Nat. Struct. Biol. 4*, 578−585.

(5) Hegg, E. L., and Que, L. (1997) The 2-His-1-Carboxylate Facial Triad. *Eur. J. Biochem. 250*, 625−629.

(6) Eser, B. E., Barr, E. W., Frantorn, P. A., Saleh, L., Bollinger, J. M., Krebs, C., and Fitzpatrick, P. F. (2007) Direct spectroscopic evidence for a high-spin Fe(IV) intermediate in tyrosine hydroxylase. *J. Am. Chem. Soc. 129*, 11334−11335.

(7) Chow, M. S., Eser, B. E., Wilson, S. A., Hodgson, K. O., Hedman, B., Fitzpatrick, P. F., and Solomon, E. I. (2009) Spectroscopy and Kinetics of Wild-Type and Mutant Tyrosine Hydroxylase: Mechanistic Insight into O_2 Activation. *J. Am. Chem. Soc. 131*, 7685−7698.

(8) Solomon, E. I., Decker, A., and Lehnert, N. (2003) Non-heme iron enzymes: Contrasts to heme catalysis. *Proc. Natl. Acad. Sci. U.S.A. 100*, 3589−3594.

(9) Andersen, O. A., Flatmark, T., and Hough, E. (2001) High resolution crystal structures of the catalytic domain of human phenylalanine hydroxylase in its catalytically active Fe(II) form and binary complex with tetrahydrobiopterin. *J. Mol. Biol. 314*, 279−291.

(10) Solomon, E. I., Brunold, T. C., Davis, M. I., Kemsley, J. N., Lee, S.-K., Lehnert, N., Neese, F., Skulan, A. J., Yang, Y.-S., and Zhou, J. (2000) Geometric and Electronic Structure/Function Correlations in Non-Heme Iron Enzymes. *Chem. Rev. 100*, 235−350.

(11) Erlandsen, H., Bjorgo, E., Flatmark, T., and Stevens, R. C. (2000) Crystal structure and site-specific mutagenesis of pterin-bound human phenylalanine hydroxylase. *Biochemistry 39*, 2208−2217.

(12) Dickson, P. W., Jennings, I. G., and Cotton, R. G. H. (1994) Delineation of the Catalytic Core of Phenylalanine Hydroxylase. *J. Biol. Chem. 269*, 20369−20375.

(13) Andersen, O. A., Stokka, A. J., Flatmark, T., and Hough, E. (2003) 2.0 Å resolution crystal structures of the ternary complexes of human phenylalanine hydroxylase catalytic domain with tetrahydrobiopterin and 3-(2-thienyl)-L-alanine or L-norleucine: Substrate specificity and molecular motions related to substrate binding. *J. Mol. Biol. 333*, 747−757.

(14) Wasinger, E. C., Mitic, N., Hedman, B., Caradonna, J. C., Solomon, E. I., and Hodgson, K. O. (2002) X-ray Absorption Spectroscopic Investigation of the Resting Ferrous and Cosubstrate Bound Active Sites of Phentlalanine Hydroxylase. *Biochemistry 41*, 6211−6217.

(15) Loeb, K. E., Westre, T. E., Kappock, T. J., Mitic, N., Glasfeld, E., Caradonna, J. P., Hedman, B., Hodgson, K. O., and Solomon, E. I. (1997) Spectroscopic characterization of the catalytically competent ferrous site of the resting, activated, and substrate-bound forms of phenylalanine hydroxylase. *J. Am. Chem. Soc. 119*, 1901−1915.

(16) Olsson, E., Martinez, A., Teigen, K., and Jensen, V. R. (2010) Water Dissociation and Dioxygen Binding in Phenylalanine Hydroxylase. *Eur. J. Inorg. Chem.*, 351−356.

(17) Enemark, J. H., and Feltham, R. D. (1974) Principles of Structure, Bonding and Reactivity for Metal Nitrosyl Complexes. *Coord. Chem. Rev. 13*, 339−406.

(18) Rich, P. R., Salerno, J. C., Leigh, J. S., and Bonner, W. D. (1978) Spin 3−2 Ferrous-Nitric Oxide Derivative of an Iron-Containing Moiety Associated with *Neurospora crassa* and Higher Plant-Mitochondria. *FEBS Lett. 93*, 323−326.

(19) Arciero, D. M., Lipscomb, J. D., Huynh, B. H., Kent, T. A., and Munck, E. (1983) EPR and Mossbauer Studies of Protocatechuate 4,5-Dioxygenase. Characterization of a New Fe^{2+} Environment. *J. Biol. Chem. 258*, 14981−14991.

(20) Aquino, F., and Rodriguez, J. H. (2009) Accurate Calculation of Zero-Field Splittings of (Bio)inorganic Complexes: Application to an $\{FeNO\}^7$ (S = 3/2) Compound. *J. Phys. Chem. A 113*, 9150−9156.

(21) Hurst, G. C., Henderson, T. A., and Kreilick, R. W. (1985) Angle-Selected Endor Spectroscopy. 1. Theoretical Interpretation of ENDOR Shifts from Randomly Orientated Transition-Metal Complexes. *J. Am. Chem. Soc. 107*, 7294−7299.

(22) Hoffman, B. M., Martinsen, J., and Venters, R. A. (1984) General Theory of Polycrystaline ENDOR Patterns. g and Hyperfine Tensors of Arbitrary Symmetry and Relative Orientation. *J. Magn. Reson. 59*, 110−123.

(23) Tierney, D. L., Rocklin, A. M., Lipscomb, J. D., Que, L., Jr., and Hoffman, B. M. (2005) ENDOR Studies of the Ligation and Structure of the Non-heme Iron Site in ACC Oxidase. *J. Am. Chem. Soc. 127*, 7005−7013.

(24) Rocklin, A. M., Tierney, D. L., Kofman, V., Brunhuber, N. M., Hoffman, B. M., Christoffersen, R. E., Reich, N. O., Lipscomb, J. D., and Que, L., Jr. (1999) Role of the Non-heme Fe(II) Center in the Biosynthesis of the Plant Hormone Ethylene. *Proc. Natl. Acad. Sci. U.S.A. 96*, 7905−7909.

(25) Yang, T. C., Wolfe, M. D., Neibergall, M. B., Mekmouche, Y., Lipscomb, J. D., and Hoffman, B. M. (2003) Substrate Binding to NO-Ferro-Napthalene 1,2 Dioxygenase Studied by High Resolution Q-Band Pulsed ^{2}H-ENDOR Spectroscopy. *J. Am. Chem. Soc. 125*, 7056−7066.

(26) Casey, T. M., Grzyska, P. K., Hausinger, R. P., and McCracken, J. (2013) Measuring the Orientation of Taurine in the Active Site of the Non-heme Fe(II)/2-ketoglutarate-Dependent Taurine Hydroxylase Using Electron Spin Echo Envelope Modulation (ESEEM) Spectroscopy. *J. Phys. Chem. B 117*, 10384−10394.

(27) Krzyaniak, M. D., Eser, B. E., Ellis, H. R., Fitzpatrick, P. F., and McCracken, J. (2013) Pulsed EPR Study of Amino Acid and Tetrahydropterin Binding in a Tyrosine Hydroxylase Nitric Oxide Complex: Evidence for Substrate Rearrangements in the Formation of the Oxygen-Reactive Complex. *Biochemistry 52*, 8430−8441.

(28) Roberts, K. M., Tormos, J. R., and Fitzpatrick, P. F. (2014) Characterization of Unstable Products of Flavin- and Pterin-Dependent Enzymes by Continuous-Flow Mass Spectrometery. *Biochemistry 53*, 2672−2679.

(29) Atherton, N. M., and Horsewill, A. J. (1979) Proton ENDOR of $Cu(H_2O)_6^{2+}$ in $Mg(NH_4)_2(SO_2)_4.6H_2O$. *Mol. Phys. 37*, 1349−1361.

(30) Höfer, P. (1994) Distortion-Free Electron Spin Echo Envelope Modulation Spectra of Disordered Solids Obtained from Two- and Three-Dimensional HYSCORE Experiments. *J. Magn. Reson. 111*, 77−86.

(31) García-Rubio, I. S., Fittipaldi, M., Trandafir, F., and Van Doorslaer, S. (2008) A Multifrequency HYSCORE Study of Weakly Coupled Nuclei in Frozen Solutions of High-Spin Aquometmyoglobin. *Inorg. Chem. 47*, 11294−11304.

(32) Fauth, J. M., Schweiger, A., Braunschweiler, L., Forrer, J., and Ernst, R. R. (1986) Elimination of unwanted echoes and reduction of dead time in three-pulse electron spin-echo spectroscopy. *J. Magn. Reson. 66*, 74−85.

(33) Shane, J. J., Höfer, P., Reijerse, E. J., and de Boer, E. (1992) Hyperfine sublevel correlation spectroscopy (HYSCORE) of disordered solids. *J. Magn. Reson. 99*, 596−604.

(34) Gemperle, C., Aebli, G., Schweiger, A., and Ernst, R. R. (1990) Phase cycling in pulse EPR. *J. Magn. Reson. 88*, 241−256.

DOI: 10.1021/acs.biochem.5b00363
Biochemistry 2015, 54, 3759−3771

(35) Stoll, S., and Schweiger, A. (2006) EasySpin, a comprehensive software package for spectral simulation and analysis in EPR. *J. Magn. Reson. 178*, 42−55.
(36) Orville, A. M., Chen, V. J., Kriauciunas, A., Harpel, M. R., Fox, B. G., Münck, E., and Lipscomb, J. D. (1992) Thiolate Ligation of the Active Site Fe(II) of Isopenecillin N Synthase Derives from Substrate Rather Than Endogenous Cysteine. *Biochemistry 31*, 4602−4612.
(37) Brown, C. A., Pavlosky, M. A., Westre, T. E., Zhang, Y., Hedman, B., Hodgson, K. O., and Solomon, E. I. (1995) Spectroscopic and Theoretical Description of the Electronic Structure of S = 3/2 Iron-Nitrosyl Complexes and Their Relation to O_2 Activation by Non-Heme Iron Enzyme Active Sites. *J. Am. Chem. Soc. 117*, 715−732.
(38) Brown, C. D., Neidig, M. L., Neibergall, M. B., Lipscomb, J. D., and Solomon, E. I. (2007) VTVH-MCD and DFT Studies of Thiolate Binding to $\{FeNO\}^7/\{FeNO\}^8$ Complexes of Isopenecillin N Synthase. *J. Am. Chem. Soc. 129*, 7427−7438.
(39) Stoll, S., and Britt, R. D. (2009) General and efficient simulation of pulse EPR spectra. *Phys. Chem. Chem. Phys. 11*, 6614−6625.
(40) Roberts, J. E., Cline, J. F., Lum, V., Freeman, H., Gray, H. B., Peisach, J., Reinhammar, B., and Hoffman, B. M. (1984) Comparative ENDOR Study of Six Blue Copper Proteins. *J. Am. Chem. Soc. 106*, 5324−5330.
(41) Bereman, R. D., and Kosman, D. J. (1977) Stereoelectronic Properties of Metalloenzymes. 5. Identification and Assignment of Ligand Hyperfine Splittings in the Elelctron Spin Resonance Spectrum of Galactose Oxidase. *J. Am. Chem. Soc. 99*, 7322−7325.
(42) Pöppl, A., and Kevan, L. (1996) A practical strategy for determination of proton hyperfine interaction parameters in paramagnetic transition metal ion complexes by two-dimensional HYSCORE electron spin resonance spectroscopy in disordered systems. *J. Phys. Chem. 100*, 3387−3394.
(43) Schweiger, A., and Jeschke, G. (2001) *Principles of Pulse Electron Paramagnetic Resonance*, Oxford University Press, Oxford, U.K.
(44) Dikanov, S. A., and Bowman, M. K. (1995) Cross-Peak Lineshape of Two Dimensional ESEEM Spectra in Disordered S = 1/2, I = 1/2 Spin Systems. *J. Magn. Reson. A116*, 125−128.
(45) Cappillino, P. J., Miecznikowski, J. R., Tyler, L. A., Tarves, P. C., McNally, J. S., Lo, W. N., Kasibhatla, B. S. T., Krzyaniak, M. D., McCracken, J., Wang, F., Armstrong, W. H., and Caradonna, J. P. (2012) Studies of iron(II) and iron(III) complexes with fac-N_2O, cis-N_2O_2 and N_2O_3 donor ligands: Models for the 2-His 1-carboxylate motif of non-heme iron monooxygenases. *Dalton Trans. 41*, 5662−5677.
(46) McCracken, J., Cappillino, P. J., McNally, J. S., Howart, M., Krzyaniak, M. D., and Caradonna, J. P. (2015) Characterization of Water Coordination to Ferrous Nitrosyl Complexes with *fac*-N_2O, cis-N_2O_2 and N_2O_3 Donor Ligands, *Inorg. Chem.*, submitted for publication.
(47) Quintanar, L., Yoon, J., Aznar, C. P., Palmer, A. E., Andersson, K. K., Britt, R. D., and Solomon, E. I. (2005) Spectroscopic and Electronic Structure Studies of the Trinuclear Cu Cluster Active Site of the Multicopper Oxidase Laccase: Nature of its Coordination Unsaturation. *J. Am. Chem. Soc. 127*, 138232−113845.
(48) Ye, S., Price, J. C., Barr, E. W., Green, M. T., Bollinger, J. M., Jr., Krebs, C., and Neese, F. (2010) Cryoreduction of the NO-adduct of Taurine:α-ketoglutarate Dioxygenase (TauD) Yields an Elusive $\{FeNO\}^8$ Species. *J. Am. Chem. Soc. 132*, 4739−4751.
(49) Martinie, R. J., Livada, J., Chang, W., Green, M. T., Krebs, C., Bollinger, J. M., and Silakov, A. (2015) Experimental Correlation of Substrate Position with Reaction Outcome in the Aliphatic Halogenase, SyrB2. *J. Am. Chem. Soc. 137*, 6912−6919.
(50) Chiou, Y.-M., and Que, L. (1995) Model Studies of a-Ket Acid-Dependent Nonheme Iron Enzymes: Nitric Oxide Adducts of $[Fe^{II}(L)(O_2CCOPh)](ClO_4)$ Complexes. *Inorg. Chem. 34*, 3270−3278.
(51) Pohl, K., Weigardt, K., Nuber, B., and Weiss, J. (1987) Preparation and Magnetism of the Binuclear Iron(II) Complexes $[\{Fe(C_9H_{21}N_3)X_2\}_2]$ (X = NCS, NCO, N_3) and their Reaction with NO. Crystal Styructures of $[\{Fe(C_9H_{21}N_3)(NCS)_2\}_2]$ and $[Fe\{C_9H_{21}N_3)(NO)(N_3)_2]$. *J. Chem. Soc., Dalton Trans.*, 187−192.
(52) Ray, M., Golombek, A. P., Hendrich, M. P., Yap, G. P. A., Liable-Sands, L. M., Rheingold, A. L., and Borovik, A. S. (1999) Structure and Magnetic Properties of Trigonal Bipyramidal Iron Nitrosyl Complexes. *Inorg. Chem. 38*, 3110−3115.
(53) Han, A. Y., Lee, A. Q., and Abu-Omar, M. M. (2006) EPR and UV-vis studies of the nitric oxide adducts of bacterial phenylalanine hydroxylase: Effects of cofactor and substrate on the iron environment. *Inorg. Chem. 45*, 4277−4283.
(54) Ellis, H. R., Daubner, S. C., and Fitzpatrick, P. F. (2000) Mutation of Serine 395 of Tyrosine Hydroxylase Decouples Oxygen-Oxygen Bond Cleavage and Tyrosine Hydroxylation. *Biochemistry 39*, 4174−4181.
(55) Kemsley, J. N., Wasinger, E. C., Datta, S., Mitic, N., Acharya, T., Hedman, B., Caradonna, J. C., Hodgson, K. O., and Solomon, E. I. (2003) Spectroscopic and Kinetic Studies of PKU-Inducing Mutants of Phenylalanine Hydroxylase: Arg158Gln and Glu280Lys. *J. Am. Chem. Soc. 125*, 5677−5686.

DOI: 10.1021/acs.biochem.5b00363
Biochemistry 2015, 54, 3759−3771